Journal of Molecular Catalysis A: Chemical 381 (2014) 26–37

Contents lists available at ScienceDirect

Journal of Molecular Catalysis A: Chemical

journal homepage: www.elsevier.com/locate/molcata

Effect of Cu content on the surface and catalytic properties of Cu/ZrO_2 catalyst for ethanol dehydrogenation

I.C. Freitas[a], S. Damyanova[b], D.C. Oliveira[c], C.M.P. Marques[d], J.M.C. Bueno[a,*]

[a] Departamento de Engenharia Química, Universidade Federal de São Carlos, C.P. 676, 13565-905 São Carlos, São Paulo, Brazil
[b] Institute of Catalysis, Bulgarian Academy of Science, 1113 Sofia, Bulgaria
[c] Laboratório Nacional de Luz Síncrotron, C.P. 6192, 13083-970 Campinas, São Paulo, Brazil
[d] Departamento de Química, Universidade Federal de São Carlos, C.P. 676, 13565-905, São Carlos, São Paulo, Brazil

ARTICLE INFO

Article history:
Received 24 July 2013
Received in revised form
26 September 2013
Accepted 29 September 2013
Available online xxx

Keywords:
Ethanol dehydrogenation
Ethyl acetate
Acetaldehyde
Cu catalysts
Characterization

ABSTRACT

ZrO_2-supported Cu catalysts with different Cu content (5–30 wt.%) were prepared by impregnation method. The effect of Cu content on the structure, surface and catalytic properties of Cu/ZrO_2 catalysts in the reaction of ethanol conversion was studied. The physicochemical characterization of the calcined and reduced samples was carried out by: N_2 adsorption–desorption isotherms, N_2O titration, XRD, XPS, TPR and DRFTS of CO adsorption. It was observed that the increase of Cu content leads to decrease of the apparent copper metal dispersion caused by the strong agglomeration of the metal particles. The selectivity to different reaction products was connected with the electronic properties of the catalysts defined by the copper particle size and the interface at metal-oxide support. The highest selectivity to ethyl acetate over samples with Cu content ≥10 wt.% was assigned to the high density of basic sites of O^{2-} ions and more heterogeneous distribution of copper species (Cu^0/Cu^+) defined by DRIFTS of CO adsorption and XPS.

1. Introduction

The reason for specifically studying the dehydrogenation of ethanol is that ethanol could be one of the future feedstock of the chemical industry. The production of ethanol from cellulosic residues will generate a large supply of bioethanol all over the world in the next decades, which will be used as a gasoline substitute or additive. The annual amount of bioethanol produced currently exceeds 50 million tons per year and is increasing. Taking into account this future large availability of bioethanol, the use of ethanol as a feedstock for the chemical industry can also be foreseen [1]. The last decades there is an increased interest in the ethanol chemistry for production of different chemicals such as ethyl acetate, acetaldehyde, hydrogen, and others. Ethyl acetate produced from ethanol has a low toxicity and it is broadly employed as a solvent in many industrial products such as paints, adhesives and coatings, as a green alternative, eliminating the use of aromatic compounds.

Different routes have been proposed for the direct synthesis of ethyl acetate from ethanol: dehydrogenative and oxidative process. A variety of heterogeneous catalytic systems with gold-based catalysts, able to oxidize primary alcohols, have been intensively investigated [2–6]. The synthesis route of ethyl acetate from ethanol dehydrogenation becomes an attractive process, because the process is relatively simple, non-corrosive and less toxic, and needs only one feedstock of ethanol. Different catalytic systems have been applied for dehydrogenation of ethanol using Cu and Pd-based catalysts supported on different carriers [7–12]. Copper-based catalysts have been successfully employed for the selective conversion of ethanol to ethyl acetate or acetaldehyde [13,14]. The best results for selective conversion to ethyl acetate have been achieved with ZrO_2-supported copper catalysts [9,10,15–19].

Some studies have shown that the support play a very important role in the formation of by-products in the reaction of selective ethanol conversion. Using Cu/ZrO_2 and Cu/SiO_2 catalysts it was suggested that the condensation reaction between ethanol and acetaldehyde occurs on the support in Cu/ZrO_2, whereas it occurs on the copper surface in Cu/SiO_2 [15]. It was demonstrated [8] that the palladium catalysts supported on SnO_2 or ZnO carriers are much more selective to ethyl acetate than on Al_2O_3 or SiO_2 ones. The effect of the support surface over the change of catalytic activity of Cu catalysts supported on different carriers was also studied in our group [20]. Studying the effect of the active sites on the selective

* Corresponding author at: Laboratório de Catalise, Departamento de Engenharia Química, Universidade Federal de São Carlos, C.P. 676, 13565-905 São Carlos, SP, Brazil. Tel.: +55 1633518439; fax: +55 1633518466.
E-mail address: jmcb@power.ufscar.br (J.M.C. Bueno).

1381-1169/$ – see front matter © 2013 Elsevier B.V. All rights reserved.
http://dx.doi.org/10.1016/j.molcata.2013.09.038

conversion of ethanol, it was suggested that Cu catalyst supported on ZrO_2 exhibits high selectivity to ethyl acetate while that supported on SiO_2 has high selectivity to acetaldehyde formation. Inui et al. [7] have shown that the treatment of Cu—Zn—Zr—Al—O catalyst with alkaline carbonate solutions leads to increase of the selectivity to ethyl acetate in the reaction of ethanol conversion; the post-treatment was more effective than the pre-treatment. The same authors also suggested that the active center of the formation of hemiacetal of acetaldehyde and ethanol exists on metal oxides not on copper metal.

The main physico-chemical properties, which determine the behavior of the oxides in the condensation reaction, still remain unknown. It is also not clear which species, ethanol or ethoxide, are involved in this reaction. Recently, it was suggested that the spillover phenomenon might occur during this synthesis [10]. However, more experimental observations are needed in order to prove it.

There is a few information in the literature [9,14,17] about the influence of Cu content on the behaviors of supported Cu catalysts in the ethanol dehydrogenation reaction. Copper catalysts supported on rice husk ash prepared by incipient wetness impregnation and the effects of both metal copper loading (1–15 wt.%) and calcination temperature on the surface structure and catalytic properties in ethanol dehydrogenation have been investigated [14]. It was shown, that the ethanol conversion and turnover frequency (TOF) has a little dependence on the copper content. However, other authors were concluded [17] that the highest ethanol conversion, and the highest space-time yield of ethyl acetate were achieved for $Cu/ZnO—ZrO_2—Al_2O_3$ catalyst at Cu content of 70 mol.%. The effect of molar ratio of copper to zirconium in Cu/ZrO_2 catalysts on the direct transformation of ethanol to ethyl acetate was investigated [9]. The highest ethanol conversion and selectivity to ethyl acetate was observed at molar Cu/Zr ratio of 1.

The aim of the present work is to study the effect of Cu content (5–30 wt.%) on the structure, electronic and catalytic properties of ZrO_2-supported Cu catalysts in the reaction of ethanol conversion. The study of the physicochemical properties will give sight on the metallic character of supported copper species and the acid-base properties of the catalyst surface that affect both, the catalytic activity and the product selectivity over Cu/ZrO_2 catalysts. This is important for improving the catalyst performance and for designing of new catalysts for dehydrogenation of ethanol. Clarification of the formation of by-products in the ethanol conversion reaction and development of the reduction of the by-products based on the formation route is important for industrial process.

The physicochemical characterization of the samples was carried out by: N_2 adsorption–desorption isotherms, N_2 titration, X-ray diffraction (XRD), X-ray photoelectron spectroscopy (XPS), diffuse reflectance Fourier transform infrared spectroscopy (DRIFTS) of CO adsorption and temperature-programmed reduction (TPR).

2. Experimental

2.1. Sample preparation

ZrO_2 support was prepared by calcination of zirconium hydroxide (from Aldrich) at 773 K in air for 4 h. Zirconia-supported Cu catalysts with different Cu content were prepared by incipient wetness impregnation of support with a solution of $Cu(NO_3)_2{\cdot}2.5H_2O$ (Aldrich 98%) in methanol. Bulk CuO was prepared according to the Ref. [21]. The solids were dried at 383 K and calcined at 773 K in an air flow for 12 and 5 h, respectively. The samples were denoted as xCu/ZrO_2, where x is the theoretical Cu loading corresponding to 5, 10, 20 and 30 wt.%.

2.2. Characterization

Specific surface area (S_{BET}) and pore volume (V_p) of the samples was determined from the corresponding nitrogen adsorption–desorption isotherms measured at 77 K on an apparatus Quantachrome Nova modelo 1200. The samples were previously degassed at 423 K for 2 h under vacuum.

XRD patterns of calcined and reduced samples were recorded on Rigaku DMAX 2500 diffractometer with CuKα ($\lambda = 1.54060$ Å) radiation operating at 40 kV and 40 mA. Diffraction peaks are recorded in a 2θ range between 5° and 85°. Step size of 0.02° and step scan of 10.0 s was used to identify the structure of the samples. Phase identification was carried out by comparison with JCPDF database cards.

XPS analysis of reduced samples was obtained with an SPECSLAB II (Phoibos-Hsa 3500 150, 9 channeltrons) SPECS spectrometer, with Al Kα source ($E = 1486.6$ eV) operating at 15 kV, Epass = 40 eV, 0.6 eV energy step and acquisition time of 2 s per point. The samples were placed on stainless steel sample-holders and were transferred under inert atmosphere to the XPS pre-chamber and stayed there for a 12 h in a vacuum atmosphere. The residual pressure inside the analysis chamber was smaller than 1×10^{-9} Torr. The binding energies (BE) of Cu 2p, Zr 3d, O 1s, Cu LMM and C 1s were referenced to the C 1s peak, at 284.5 eV, providing accuracy within ±0.2 eV. All samples were reduced in a furnace from room temperature to desired temperature according to H_2-TPR behavior at 10 K/min, staying at the 573 K for 30 min under a 200 ml/min flow rate of 5%H_2/He, and then cooled to room temperature to proceed subsequent analysis. X-ray induced Auger electron spectra of reduced samples in the kinetic region of 928–902 eV were also obtained. The modified Auger parameter (α_{Cu}) was calculated according the Eq. (1) [22]:

$$\alpha_{Cu} = E_B + E_K \quad (1)$$

where E_B is the binding energy of Cu 2p core level and E_K is the kinetic energy of the Cu LMM Auger electron.

TPR profiles were recorded on a Micromeritics Pulse Chemisorb 2705 fitted with a thermo conductivity detector (TCD). In order to remove surface contaminants, the sample (0.05 g) loaded in a quartz reactor was pretreated at 423 K in a He stream for 1 h. After cooling to room temperature a flow of 5% H_2/N_2 (30 ml/min) was passed through the sample and the temperature was raised at a rate of 10 K/min up to 773 K while the TCD signal was recorded. A cooling trap placed between the sample and the detector retained the water formed during the reduction process.

In the same TPR apparatus described above, N_2O titration was used to determine the surface area of dispersed metallic Cu. This method consists of two ways: (i) oxidation of Cu^0 to Cu_2O using N_2O as oxidation agent and (ii) temperature programmed reduction of surface Cu_2O species. The Cu/ZrO_2 samples were pre-reduced up to 523 K and after that were cooled to 303 K and exposed to 1% N_2O/He (30 ml/min) for 10 min. A second H_2-TPR by increasing the temperature up to 773 K at a rate of 10 K/min under 5% H_2/He was acquired. The hydrogen consumption was used to calculate the amount of oxygen deposited after N_2O titration. A total of 1.46×10^{19} Cu atoms/m^2 and a stoichiometry of $2Cu/H_2$ were used [23]. The Cu surface area (SA_{Cu}) was calculated on the basis of the following relationship (Eq. (2)):

$$SA_{Cu} = 6.4955 \times 10^{-2} \times C \times D \quad (m^2/g_{cat}) \quad (2)$$

where C is Cu content (%) and D is metallic (Cu^0) dispersion (%).

By assuming a spherical shape of the copper metal particles, the average metal copper particle size (d_{Cu}) was determined by the following expression [24]:

$$d_{Cu}(nm) = \frac{6000}{SA_{Cu} \times \rho_{Cu}} \quad (3)$$

where ρ_{Cu} is the copper density of 8.92 g/cm^3.

The DRIFT spectra of adsorbed CO were recorded using a Thermo Nicolet 4700 Nexus FTIR spectrophotometer with MCT detector and a reactor cell Spectra Tech with CaF_2 windows (DRIFT HTHV cell). IR spectra were collected in 64 scans at 4 cm^{-1} resolution. Before reduction the samples were dried at 473 K in a He flow during 1 h. Then the catalysts were reduced at 573 K in a flow of 25% H_2/He mixture for 2 h. The CO was introduced for 1 s and adsorbed at 323 K at CO pressure of 20 Torr. Temperature-programmed desorption (TPD) of adsorbed CO was carried out in flowing He (30 ml/min) with a heating rate of 10 K/min.

2.3. Catalytic test reaction

Activity and selectivity of the catalysts in the reaction of ethanol conversion were carried out in a continuous-flow, tubular fixed-bed quartz reactor (10 mm i.d.) with catalyst weight of 0.5 g over the temperature range of 473–548 K at atmospheric pressure. The reaction was carried out at contact time of $W/F = 19$ min, where W and F correspond to catalyst weight (g) and flow rate of ethanol (g/min), respectively. Samples were reduced in situ by heating in pure H_2 flow from room temperature to 573 K at 10 K/min staying at this temperature for 150 min. Ethanol (99.9%) in gas phase was fed to catalytic reactor by passing He flow of 10 ml/min. Reaction products were collected periodically and analyzed by on-line gas chromatography (Varian GC-3400 CX) with a Chromosorb 102 column. Conversion and selectivity were determined on the carbon basis products.

3. Results

3.1. Textural properties and structure

3.1.1. XRD and BET analysis

Fig. 1 shows the diffraction patterns of calcined (A) and reduced (B) Cu/ZrO_2 samples with different Cu content. For comparison the XRD of pure ZrO_2 and CuO are shown in the Fig. 1. The crystallinity of ZrO_2 synthesized in the present study is supported by sharp diffraction peaks at the respectively diffraction angles, which correspond to tetragonal structure (t-ZrO_2). The sample exhibits major peaks at $2\theta = 30.3$, 35.2, 50.6 and 60.2°, which are comparable with the standard JCPDS data (card No. 170923). There is no indication for the presence of low temperature monoclinic and high temperature cubic phases in the XRD of t-ZrO_2 (Fig. 1A). Evidence of the tetragonal symmetry might be again confirmed by the non-symmetric line shape at around $2\theta = 35°$ and 60° regions of the XRD. In the region of $2\theta = 35°$ the non-symmetric line shape is originated from the splitting between the (0 0 2) and (1 1 0) peaks situated near 2θ values of 34.63 and 35.16°, respectively. Similarly, in the region of $2\theta = 60°$, the non-symmetric peak is due to the overlapping of indexed peaks (1 0 3) and (2 1 1) situated at $2\theta = 59.3°$ and $2\theta = 60.03°$, respectively.

Bulk CuO exhibits main sharp peaks at $2\theta = 32.6$, 35.6, 38.6, 48.8, 53.6, 58.3, 61.6, 66.4, 68.1, 72.3 and 75.1° corresponding to a crystalline CuO phase with tenorite structure (JCPDS 481548) (Fig. 1A). The XRD patterns of ZrO_2-supported Cu samples with lower Cu content up to 10 wt.% Cu do not exhibit peaks characteristic of CuO species. This means that the size of CuO is beyond the detection capacity of the XRD technique. However, the increase of Cu content (to 20 and 30 wt. %) leads to the appearance of characteristic CuO peaks at $2\theta = 35$, 38.7, 49.1, 66.5, 68.0 and 74.7° in addition to the ZrO_2 peaks that means an agglomeration of the copper oxide species (Fig. 1A). The intensity of the XRD peaks of supported CuO is the highest for $30Cu/ZrO_2$. This clearly suggests the increase of the crystallinity and formation of bulk CuO at higher loadings (≥20 wt.%). The XRD of Cu/ZrO_2 samples also show that a new phase with $2\theta = 28$ and 24° is observed after supporting of the copper oxide species over t-ZrO_2 and calcination at 773 K (Fig. 1A). This could be connected with some surface transformation of t-ZrO_2 to m-ZrO_2 phase. Transformation of ZrO_2 from tetragonal to monoclinic structure takes place initially at surface regions and then develops into the bulk with increasing the reaction temperature. It was shown [25] that t-ZrO_2 nanocrystals were partially transformed into monoclinic phase at treatment temperature ≥973 K. Other authors [26] have also observed the transformation of tetragonal ZrO_2 phase to monoclinic one after its impregnation with molybdenum oxide.

The treatment of Cu/ZrO_2 under hydrogen atmosphere at 573 K leads to reduction of the copper oxide species to metallic copper (Cu^0) revealed by the XRD at $2\theta = 43$, 50 and 74° (JCPDS 04-0836), which is well visible for samples with higher Cu content ≥20 wt.% (Fig. 1B). There is a very good agreement between the XRD of reduced samples and the data from the N_2O measurements. The highest intensity of the XRD of metallic copper in Fig. 1B

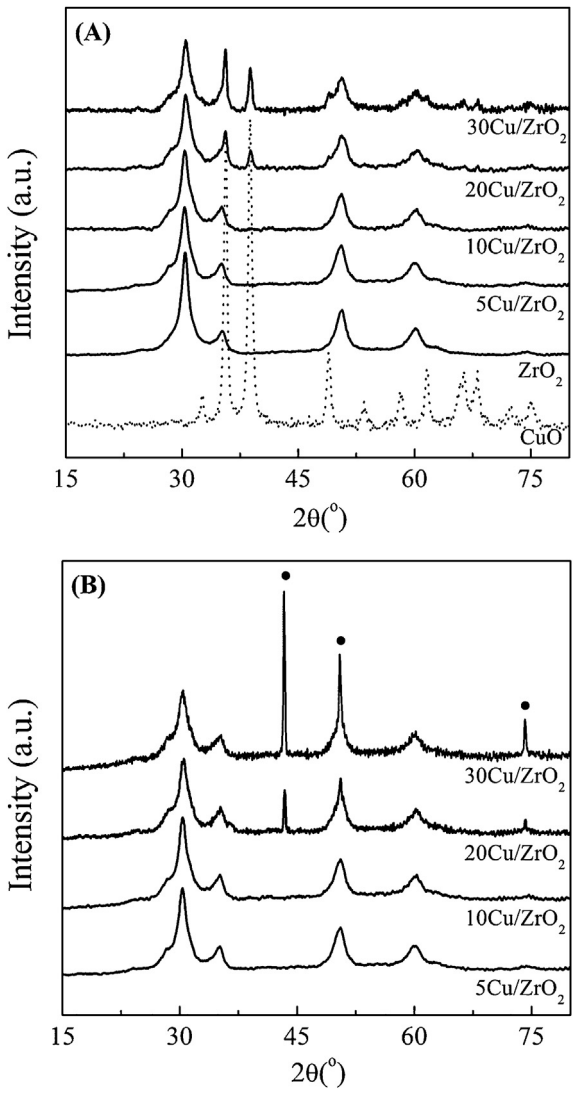

Fig. 1. XRD of calcined (A) and reduced (B) Cu/ZrO_2 samples with different Cu content; Cu^0 (●).

Table 1
Textural properties of Cu/ZrO_2 samples.

Sample	S_{BET} (m^2/g)	V_p (cm^3/g)	SA_{Cu} (m^2/g_{cat})	D_{Cu} (%)	d_{Cu} (nm)
ZrO_2	212	0.9	–	–	–
$5Cu/ZrO_2$	186	0.8	10.4	34	3.1
$10Cu/ZrO_2$	175	0.7	13.8	23	4.4
$20Cu/ZrO_2$	146	0.6	14.7	14	7.6
$30Cu/ZrO_2$	137	0.6	12.3	8	12.6

corresponds to the highest metal particle size of Cu^0 in Cu/ZrO_2 with the highest copper loading of 30 wt.% (Table 1).

Some textural characteristics of *t*-ZrO_2 and calcined Cu/ZrO_2 samples with different Cu content are listed in Table 1. The metallic Cu surface area, SA_{Cu}, the apparent metallic Cu dispersion, D_{Cu}, and the metal particle size measured by N_2O are also given in the Table 1. The BET specific surface areas and pore volume of Cu/ZrO_2 samples are lower compared to those of *t*-ZrO_2 support. S_{BET} of pure zirconia is 212 m^2/g. The increase of Cu content leads to a decrease of the values of S_{BET} and V_p caused by: (i) consumption of surface hydroxyl groups of the support by reaction with the active oxide precursor up to 10 wt.% Cu and (ii) agglomeration of CuO at Cu content ≥20 wt.% and coverage of support pores. The latter is supported by the XRD spectra of calcined $20Cu/ZrO_2$ and $30Cu/ZrO_2$ samples, where there is an increase of the peak intensity of supported Cu oxide species (Fig. 1A). The highest apparent Cu^0 dispersion measured by N_2O titration is observed for Cu/*t*-ZrO_2 sample with the lowest Cu content (5 wt.%), to which corresponds the smallest metallic Cu particle size of 3.1 nm (Table 1). The lowest apparent Cu^0 dispersion is detected for $30Cu/ZrO_2$ caused by the copper agglomeration. On the other hand, the $5Cu/ZrO_2$ sample is characterized by the lowest surface metallic area, probably, due to a strong interaction between the copper oxide species and surface of zirconia carrier.

3.2. Surface properties

3.2.1. XPS analysis

The catalyst surface composition and oxidation state of the components are investigated by XPS. XPS of Cu 2p and Auger, Zr 3d and O 1s core electron levels for reduced Cu/ZrO_2 samples are shown in Fig. 2A–D, respectively. The XPS parameters are summarized in Table 2. The values of BEs of Cu $2p_{3/2}$, Zr $3d_{5/2}$ and of O 1s core electron as well as the values of the width at half maximum (FWHM) of Cu $2p_{3/2}$ are reported in Table 2. All reduced samples exhibit symmetric Cu $2p_{3/2}$ and Cu $2p_{1/2}$ main peaks with BEs values at ca. 932.5–931.9 eV and ca. 952.4 eV, respectively, and with a spin–orbit coupling energy of about 20 eV (Fig. 2A). A shakeup satellite at ca. 942 eV is not detected, which suggests the absence of Cu^{2+} species [22]. It should be noted, that there is some increase of the value of BE of Cu $2p_{3/2}$ with decrease of Cu content (from 931.9 to 932.5 eV for $30Cu/ZrO_2$ and $5Cu/ZrO_2$, respectively, Table 2), probably, caused by an electron transfer from Cu to ZrO_2. The FWHM of Cu $2p_{3/2}$ is 2.1–2.4 eV, which means the presence of at least two kinds of surface copper species in different chemical environments. Therefore, traces of other species, like Cu^+, cannot be excluded, since the BEs of Cu^+ generally overlap with those of Cu^0 in the Cu 2p core level.

To distinguish Cu^0 from Cu^+ species, having similar BE, the X-ray induced Auger electron spectra of reduced Cu/ZrO_2 samples in the kinetic region of 928–902 eV are presented in Fig. 2B. A clear difference is observed in the shapes of Cu $L_3M_{45}M_{45}$ Auger photoelectron spectra of the samples due to the specific bonding interactions at the interface between the both metal and oxide species. Peaks at 918.8–919.3 eV and at 914.6 eV (Table 2) are revealed that are assigned to Cu^0 and Cu_2O, respectively [27]. The increase of Cu content in Cu/ZrO_2 samples leads to a shift of the peak, characteristic of metallic copper species, to a higher kinetic energy of 919.3 eV for $30Cu/ZrO_2$ sample (Fig. 2B and Table 2). The values of modified Auger parameter, α_{Cu}, are 1850.8–1851.1 eV and 1846.8–1847.4 eV, which correspond to Cu^0 and Cu^+ species, respectively (Table 2). It can be concluded that the Cu^+ species is dominant on the surface of Cu/ZrO_2 sample with the lowest Cu content ($5Cu/ZrO_2$), whereas metallic copper is prevailing for samples with higher Cu content (20 and 30 wt.%). There is some equilibrium between the Cu^0 and Cu^+ species for $10Cu/ZrO_2$, being seen in Fig. 2B.

All Cu/ZrO_2 samples exhibit a spin–orbit doublet of the Zr 3d core level into $3d_{5/2}$ and $3d_{3/2}$ levels with energy gap of 2.4 eV between them and a relative intensity ratio (I $3d_{5/2}$/I $3d_{3/2}$) of 1.5 (Fig. 2C). This indicates the existence of ZrO_2-like species according to the literature data [28]. Decomposition of the spectra produces peaks attributed to the existence of two kinds of zirconium species, assigned to species I with low BE at ca.182.3 eV (Zr_I), characteristic of Zr^{4+} ions in pure ZrO_2 and species II with higher BE at ca.183.7 eV (Zr_{II}) (Table 2) due to the formation of zirconium species bound to a more electron-attractive species and formation of partially reduced $Zr^{\delta+}$ sites [28]. The fraction of Zr_I species for all samples is larger compared to that of species Zr_{II}.

The value of atomic XPS Cu/Zr ratio of reduced Cu/ZrO_2 samples increases in the following order: $5Cu/ZrO_2 > 10Cu/ZrO_2 > 20Cu/ZrO_2 > 30Cu/ZrO_2$ (Table 2). A strong increase of the XPS intensity Cu/Zr ratio is observed up to 20 wt.% Cu and no too strong with further increase of the Cu content (at 30 wt.%). The highest Cu/Zr ratio value of 1.46 for $30Cu/ZrO_2$ means a Cu enrichment on the ZrO_2 surface.

The XPS of O 1s core electrons (Fig. 2D) are broad due to overlapping contributions of lattice oxygen from zirconia and supported copper species. The broad O 1s peaks are decomposed in two peaks at the corresponding position using XPS peak splitting program (XPS Casa Software). According to the literature [29,30] there might be two types of oxygen species in the Cu/ZrO_2 system after reduction: oxygen species of ZrO_2 and/or Cu_2O (O_I) and oxygen species of Zr—OH (O_{II}), whose binding energy are at ca. 530.3 eV and at ca. 532.2 eV, respectively (Table 2).

3.2.2. DRIFT spectra of CO adsorption

DRIFT spectra of CO adsorption on reduced Cu/ZrO_2 samples in the high frequency (HF) region of 2200–2000 cm^{-1} and in the low frequency (LF) region of 1800–1200 cm^{-1} are shown in Figs. 3A–D and 4 A–D, respectively. The figures also display the spectra of temperature-programmed desorption (TPD) of CO at 373–773 K. A first inspection of the figures reveals that the distribution of the bands for all samples is quite similar. A description of the bands is shown in Table S1 (see Supplementary Material).

According to the literature data [31], in the HF spectral region the CO adsorption on copper surface exhibits IR bands associated with the linear or bridge-bonded CO species interacting with CuO, Cu_2O or Cu^0 sites [31]. In general, the bands related to Cu^+—CO carbonyls are revealed at 2116–2111 cm^{-1}, while the bands assigned to CO adsorbed on Cu^0 species are detected at ≤2100 cm^{-1} [31]. Practically, there is no difference in the copper spectral region of the IR spectra of reduced Cu/ZrO_2 samples being seen in the Fig. 3A–D. Well defined band with a maximum at ca. 2097 cm^{-1}

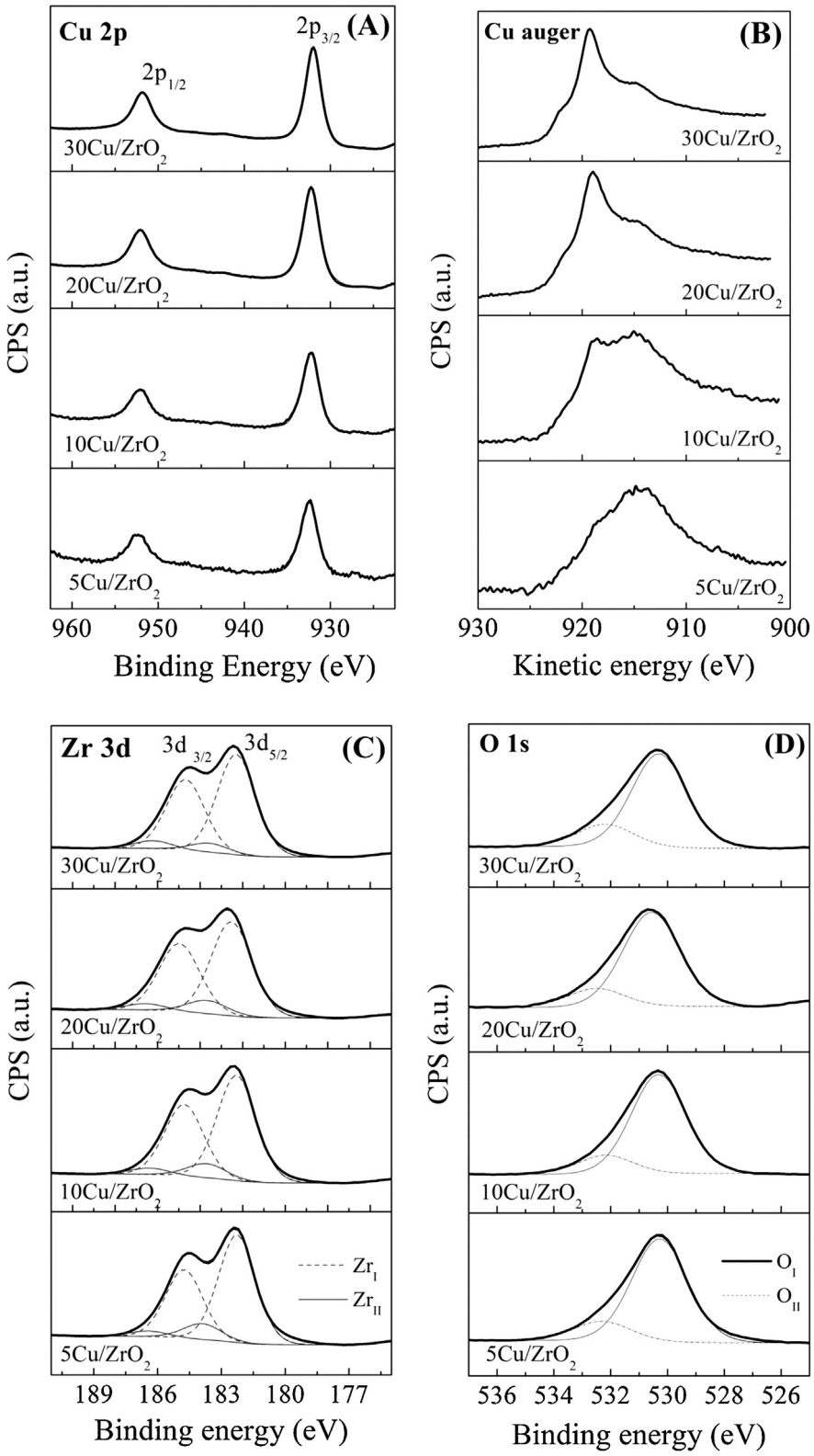

Fig. 2. XPS of Cu 2p (A), Cu Auger (B), Zr 3d (C) and O 1s core level (D) for reduced Cu/ZrO_2 samples.

in the HF region is observed for all samples, due to the surface Cu^0—CO carbonyls. According to the literature data [31], when the copper is highly dispersed on the surface, the Cu^0—CO carbonyls species can be adsorbed at the same frequency, like that of Cu^+—CO ones. The highest Cu^0 dispersion is observed for $5Cu/ZrO_2$ as was shown by the N_2O titration data (Table 1). The both species can be better distinguished by their thermal stability criterion in the TPD of CO (Fig. 3A–D: the surface Cu^0—CO carbonyls are easily destroyed with increasing the temperature, while Cu^+ cations form more stable surface carbonyls. The adsorbed carbonyl species for Cu/ZrO_2 samples with Cu content of 5–20 wt.% are decomposed at higher temperature (at 423 K) compared to that with the highest

Table 2
XPS characteristics of reduced Cu/ZrO2 samples.

Sample	Cu 2p3/2	Cu Auger	αCu (eV)	Zr 3d5/2 (eV)		O 1s (eV)		Cu/Zr
	(eV)	(eV)		ZrI species	ZrII species	OI species	OII species	
5Cu/ZrO2	932.5 (2.4)[a]	914.7	1847.2	182.3 (87)[b]	183.8 (13)	530.3 (84)[b]	532.3 (16)	0.06
10Cu/ZrO2	932.3 (2.4)	918.8/914.7	1847.3/1850.8	182.3 (88)	183.7 (12)	530.3 (84)	532.2 (16)	0.15
20Cu/ZrO2	932.2 (2.3)	918.9/914.6	1847.5/1851.1	182.4 (88)	183.7 (12)	530.4 (83)	532.3 (17)	1.05
30Cu/ZrO2	931.9 (2.1)	919.3/914.6	1846.8/1851.1	182.3 (92)	183.6 (8)	530.3 (80)	532.2 (20)	1.46

[a] FWHM;
[b] Percent.

Cu concentration of 30 wt.% (at 373 K). It means that in addition to the presence of Cu^0 there is a fraction of Cu species with a lower electron density in Cu/ZrO_2 samples with Cu content ≤20 wt.%.

The CO adsorption capacity on ZrO_2 support as well as the position and intensities of the IR bands in the LF region of 1800–1200 cm^{-1} depend on the Cu content, being seen in Fig. 4A–D. The different surface species formed upon CO molecule adsorption give information on the existence of surface basic sites (low basic OH groups and *cus* O^{2-} centers) or acid-base pair sites (*cus* Zr^{4+}—O^{2-} centers) [32]. Relatively well resolved bands at 1604, 1576, 1449, 1415, 1360 and 1326 cm^{-1} with shoulders at ca. 1790, 1638, 1522, 1467 and 1225 cm^{-1} are observed for $5Cu/ZrO_2$ sample, which are related to different CO bonded species caused by the presence of acid-base sites. The formation of bridged bidentate carbonate species (*b*-HCO_3^-) is negligible, revealed by the shoulders at ca.1638 and at ca.1225 cm^{-1}. The hydrogen carbonate species are formed by adsorption of CO on basic hydroxyl groups. In addition, the thermal stability of the hydrogen carbonates is very limited, being practically eliminated at 423 K (Fig. 4A).

The bands at ca. 1604–1576 and 1326 cm^{-1} and at ca. 1360 cm^{-1} can be assigned to bidentate (*b*-CO_3^{2-}) and monodentate (*m*-CO_3^{2-}) carbonates species, respectively. According to the literature [33,34] the surface bidentate carbonate complexes involve acid-base pair sites (*cus* Zr^{4+}—O^{2-} centers), whereas the monodentate carbonates are formed over *cus* O^{2-} centers of high basicity.

The bands at 1449 and 1415 cm^{-1} could be related to monodentate carbonate species on the basis of their small spectral separation. However, considering the strong thermal resistance of the both species (up to 573 K) and the rather low separation between the two C—O stretching modes these species correspond to planar polydentate bridging carbonate complex (*p*-CO_3^{2-}), where the three carbonate oxygen are bonded to metal ions [35]. Therefore, the formation of polydentate carbonate species means a large amount of close spaced *cus* Zr^{4+} cationic centers on the surface of $5Cu/ZrO_2$ sample (Fig. 4A). Increasing the Cu content in the samples leads to a small shift in the position of the both bands, but the ratio between them is significantly changed. Traces of ionic bicarbonate species (*i*-HCO_3^-) are observed at ca.1690 cm^{-1}.

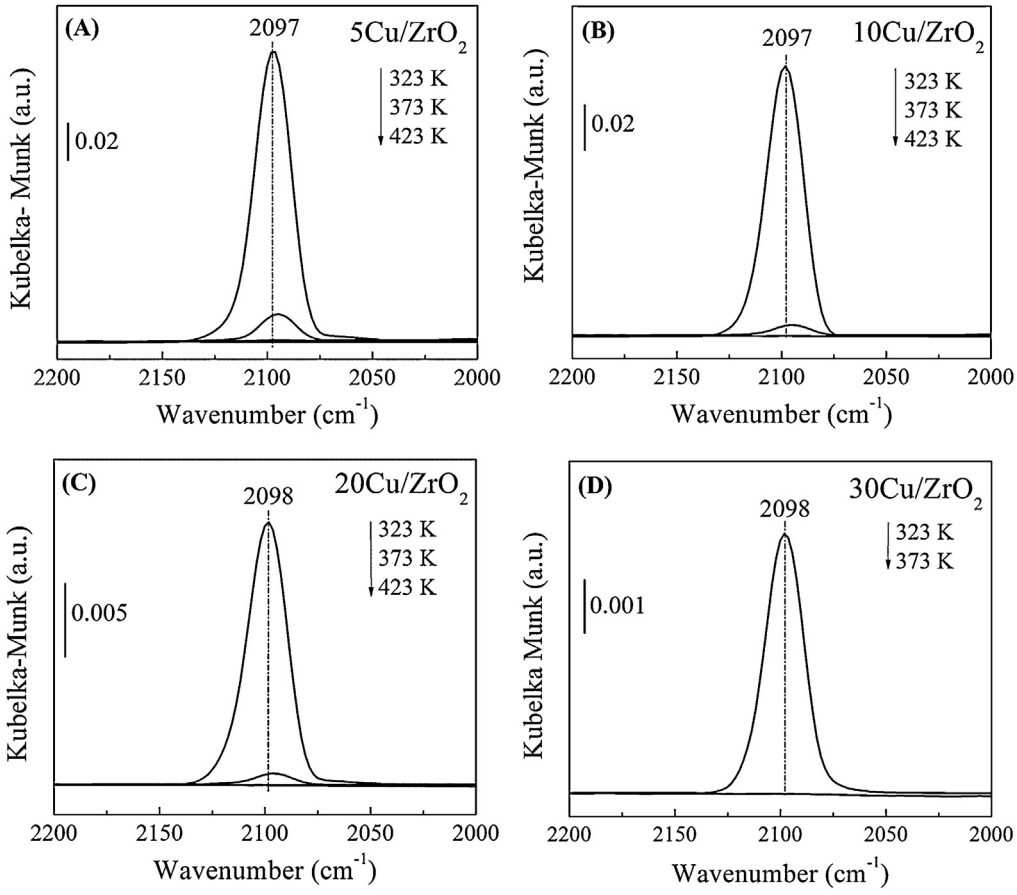

Fig. 3. FTIR spectra of CO adsorption in the HF region of 2200–2000 cm^{-1} on reduced Cu/ZrO_2 samples: $5Cu/ZrO_2$ (A), $10Cu/ZrO_2$ (B), $20Cu/ZrO_2$ (C) and $30Cu/ZrO_2$ (D).

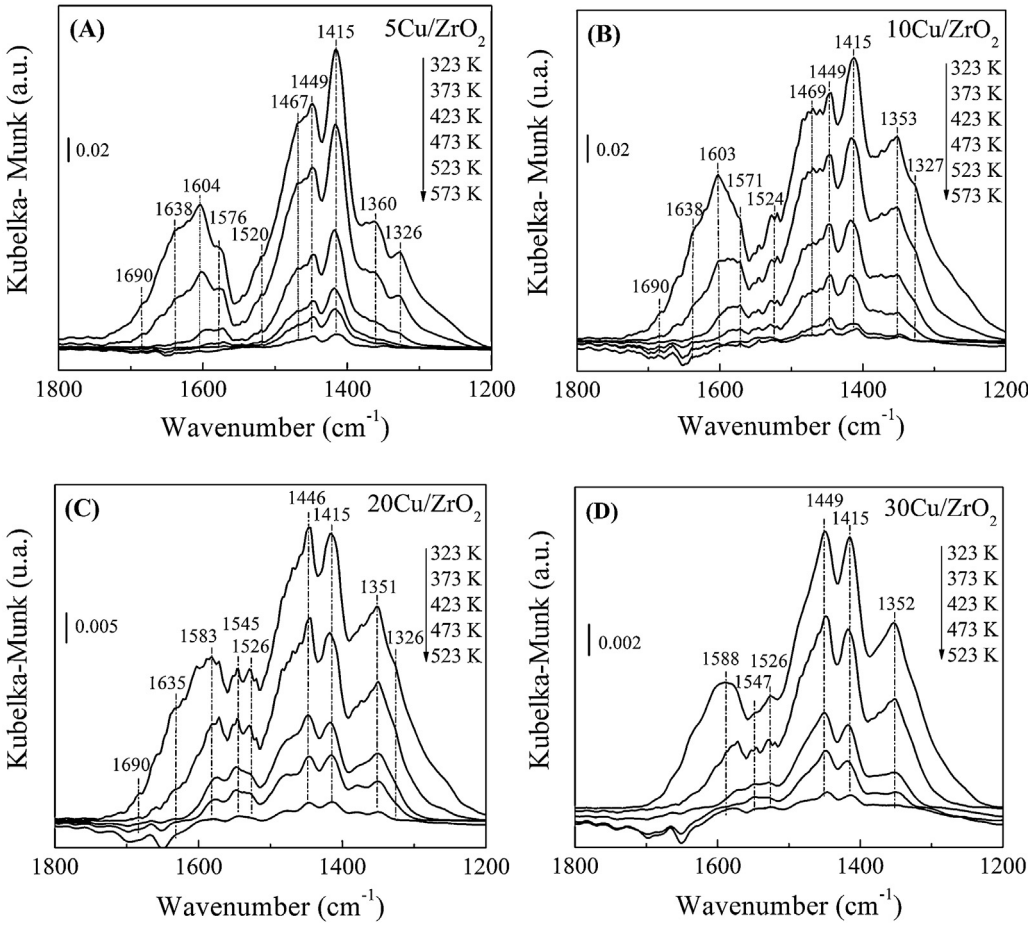

Fig. 4. FTIR spectra of CO adsorption in the LF region of 1800–1200 cm^{-1} on reduced Cu/ZrO_2 samples: $5Cu/ZrO_2$ (A), $10Cu/ZrO_2$ (B), $20Cu/ZrO_2$ (C) and $30Cu/ZrO_2$ (D).

The adsorption capacity of CO on the Cu/ZrO_2 samples in the LF region (Fig. 4) increases with increasing the surface area of the samples, suggesting that the surface density of adsorption sites increases with decreasing the Cu content, i.e. when more bulk zirconia surface is exposed to CO adsorption. The latter is well visible for $5Cu/ZrO_2$ sample.

Predominantly weakly bonded bicarbonate species are formed on the surface of $5Cu/ZrO_2$ and $10Cu/ZrO_2$. This would be related to a higher fraction of the exposed free basic hydroxyl groups at the surface of *t*-ZrO_2 surface. The fraction of this species is decreased with increasing the Cu content ≥20 wt.%, due to the consumption of OH groups by Cu species. The fraction of monodentate (*m*-CO_3^{2-}) carbonates caused by the strongly basic surface O^{2-} anions increases with increasing the Cu content from 5 up to 10 wt.% revealed by the increase of the band intensity at ca. 1360 cm^{-1} (Fig. 7A and B). It should be noted that the total CO adsorption capacity over ZrO_2 surface for Cu/ZrO_2 samples with 20 and 30 wt.% Cu is significantly lower compared to that for samples with lower copper content that is caused by covering the carrier surface with supported Cu species.

The thermal stability of adsorbed CO on different samples, illustrated in Fig. 4A–D is not similar. This could be related to the different concentration of the species on the surface of the solids, but their nature is identical according to the FTIR spectra. A decrease of the band intensity and a shift of the band position is observed with the temperature increase of CO desorption. Comparing the FTIR spectra of all samples it is seen that the bicarbonate and monodentate species for sample with Cu content of 30 wt.% decomposes at relatively low temperature (below 573 K), i.e. they are the least stable to thermal decomposition. The CO adsorption capacity in Cu/ZrO_2 sample with lower Cu content of 5 and 10 wt.% is retained to a significantly higher temperature (up to 573 K) than that for samples with higher Cu loading (up to 523 K for $20Cu/ZrO_2$ and $30Cu/ZrO_2$). The strong bonded CO on ZrO_2 surface is revealed by the presence of the bands ca. 1450 and 1415 cm^{-1} assigned to *p*-CO_3^{2-} species caused by the presence of strong Lewis acid sites due to the closely spaced *cus* Zr^{4+} sites. [36]. The abundant exposed Zr^{4+} species in $5Cu/ZrO_2$ sample, characteristics of high strength Lewis acid sites, is confirmed by the lowest atomic XPS Cu/Zr ratio (Table 2).

3.3. Reductive properties

3.3.1. TPR

Temperature-programmed reduction experiments were performed to evaluate the reducibility of ZrO_2-supported CuO catalysts. This technique is suitable for studying low- loaded and highly dispersed systems whose characteristics are beyond the limits of detectability by other direct structural analysis methods, like XRD. Fig. 5 shows the TPR profiles of calcined Cu/ZrO_2 samples. For comparison, the TPR of bulk CuO is added in the Fig. 5. To facilitate the description of TPR profiles, the TPR patterns are divided in two main temperature regions: low-temperature region I (423–493 K) and high-temperature region II (503–570 K). The calculated hydrogen consumption and the maximum of TPR peaks (T_{max}) of the samples in the both temperature regions are listed in Table 3. The reduction temperatures in regions I and II should be related to the reduction of supported Cu oxide species in different interaction with the carrier surface as well as to the different particle size, respectively to the different Cu content. In the case of

Table 3
TPR characteristics of Cu/ZrO_2 samples with different Cu content.

Sample	Region I		Region II		Total H_2 consumption ($\mu mol/g_{cat}$)
	T_{max} (K)	H_2 consumption ($\mu mol/g_{cat}$)	T_{max} (K)	H_2 consumption ($\mu mol/g_{cat}$)	
$5Cu/ZrO_2$	449	36.8	–	–	36.8
$10Cu/ZrO_2$	456	60.6	–	–	60.6
$20Cu/ZrO_2$	457	59.6	506	51.9	111.5
$30Cu/ZrO_2$	445	44.9	515	118.3	163.2
bulk CuO	–	–	558	281.4	281.4

weak interaction, the copper species can be easily reduced at lower temperature than in the case of a strong interaction. The intensity and position of the peaks in regions I and II depend on the Cu content. The both low Cu-loaded samples, $5Cu/ZrO_2$ and $10Cu/ZrO_2$, practically have a similar shape of the TPR profiles, since they show signals in common that is not evident for the samples with higher Cu content (20 and 30 wt.%) (Fig. 5). These samples exhibit hydrogen consumption in the temperature region I only (Table 3). A broad peak with a maximum at 449 K and a shoulder at ca. 462 K appear in the TPR profile of Cu/ZrO_2 sample with the lowest Cu content (5 wt.%). This suggests a heterogeneous distribution of copper oxide species over ZrO_2 surface corresponding to the reduction of well dispersed copper oxide species in a moderated and in a strong interaction with the support, respectively. Increasing the Cu content to 10 wt.% leads to a slight shift of the maximum of TPR peak to 456 K and to an increase of its intensity. It is interesting to note, that the shoulder at 462 K is disappeared in the TPR profile of $10Cu/ZrO_2$. It can be concluded that the TPR data for Cu/ZrO_2 samples with 5–10 wt.% Cu are in agreement with the results of XRD and N_2O measurements (Table 1).

High-loaded Cu samples (20 and 30 wt.% Cu) exhibit hydrogen uptakes in the both temperature regions I and II, as the fraction of hydrogen consumption in the second one is greatly affected by the amount of Cu (Fig. 5 and Table 3). Two strong peaks with maxima at 457 and 506 K are appeared in the TPR profile of $20/ZrO_2$ sample. A shoulder in the higher-temperature side of the first peak at about 466 K is also revealed. In the TPR profile of the sample with the highest Cu content (30 wt.%) the peak in the region II significantly grows and shifts to a higher temperature of 515 K, while the peak intensity in the region I decreases and shifts to a lower temperature. This suggests that the peak in high temperature region increases at the expense of the peak in lower temperature region. It can be concluded that $20Cu/ZrO_2$ and $30Cu/ZrO_2$ exhibit higher total hydrogen consumption compared to that of the samples with lower Cu content (≤10 wt.%, Table 3).

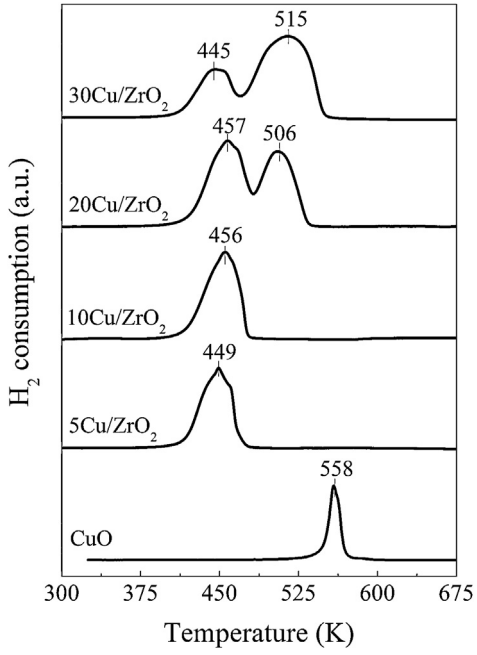

Fig. 5. TPR profiles of Cu/ZrO_2 samples with different Cu content.

Bulk CuO exhibits a sharp TPR peak at 558 K. However, the reduction temperature of CuO significantly decreases after its supporting on the surface of t-ZrO_2, being seen in Fig. 5. Similar reduction behavior of the Cu/ZrO_2 system has been observed by other authors [37], who reported that the lower temperature peaks are due to the presence of highly dispersed CuO with an octahedral environment of Cu^{2+} ions, while the higher temperature peaks are assigned to reduction of large CuO crystallites. According to Ref. [37] the highly dispersed copper species include both isolated Cu^{2+} ions in a moderate and in a strong interaction with the support and also small two-dimensional clusters. The TPR peak in the higher temperature region II is attributed to large three-dimensional CuO clusters. The broadening of the TPR peak in region II and its shifting to higher temperatures is related to the increase of the crystallinity of CuO with increasing the Cu content, being confirmed by the data from the XRD and N_2O measurements. The highest copper particle size is observed for $30Cu/ZrO_2$, while the apparent Cu^0 dispersion and the surface metallic area are decreased due to the strong agglomeration of Cu^0 (Table 1).

3.4. Catalytic performance of Cu/ZrO_2 catalysts in ethanol conversion reaction and relation to physicochemical properties

The effect of the reaction temperature as well as of the Cu content on the ethanol conversion, activity and product selectivity are listed in Table 4. The main reaction products are acetaldehyde (AcH) and ethyl acetate (EtOAc). By-products of ethanol reaction are also formed, which are: methyl ethyl ketone (MEK), crotonaldehyde (CROT), propanone (PROP), ethene (ETE) and others, like CO and CO_2.

The values of ethanol conversion for all Cu catalysts increase with increasing the reaction temperature from 473 to 548 K (Table 4). However, there is no significant influence of the Cu content on the change of ethanol conversion at each reaction temperature. It should be noted, that the conversion is slightly increased for catalysts with 10 and 20 wt.% Cu compared to that for samples with 5 and 30 wt.% Cu. The lowest ethanol conversion values at all reaction temperatures are observed for catalyst with the lowest Cu content ($5Cu/ZrO_2$).

Fig. 6 shows changes of the conversion of ethanol (A) and selectivity to acetaldehyde, ethyl acetate and to products of aldol condensation (B) as a function of the reaction temperature. It should be noted, that the selectivity to ethyl acetate for all catalysts is higher compared to the selectivity to acetaldehyde at all reaction temperatures. The highest selectivity to ethyl acetate is observed for $20Cu/ZrO_2$ and $10Cu/ZrO_2$ catalysts, followed by that of $30Cu/ZrO_2$ (Fig. 6B). The catalyst with the lowest Cu content exhibits the lowest ethyl acetate selectivity. The selectivity to ethyl

Table 4
Effect of copper content on the behavior of Cu/ZrO_2 catalysts in ethanol conversion at different reaction temperatures.

$T_{reac.}$ (K)	Catalyst	X_{EtOH} (%)	Selectivity (%)							Quantity (mol)		Ratio H_2O/PCD
			AcH	EtOAc	MEK	CROT	PROP	ETE	Others[a]	H_2O	PCD	
473	$5Cu/ZrO_2$	27.9	21.0	71.2	2.7	5.0	0.1	0.0	0.0	914.3	506.3	1.8
	$10Cu/ZrO_2$	33.3	16.6	75.0	2.7	4.7	0.4	0.6	0.1	1069.0	664.9	1.6
	$20Cu/ZrO_2$	31.9	16.8	75.5	2.7	4.3	0.3	0.4	0.0	787.3	436.6	1.8
	$30Cu/ZrO_2$	30.9	20.1	73.6	2.8	3.0	0	0.5	0.1	588.7	279.8	1.9
498	$5Cu/ZrO_2$	45.8	18.3	70.9	3.2	6.9	0.4	0.0	0.3	1725.4	675.6	2.5
	$10Cu/ZrO_2$	50.7	14.1	78.3	3.0	3.8	0.4	0.0	0.4	1269.5	571.9	2.2
	$20Cu/ZrO_2$	51.1	14.6	79.1	2.8	2.8	0.4	0.0	0.3	1116.8	496.6	2.2
	$30Cu/ZrO_2$	49.6	16.7	76.5	2.8	3.3	0.3	0.2	0.2	1138.6	483.2	2.3
523	$5Cu/ZrO_2$	64.3	16.8	72.7	3.5	5.0	1.1	0.1	0.8	2835.0	776.2	3.6
	$10Cu/ZrO_2$	68.4	12.5	79.5	2.7	2.9	1.1	0.3	1.0	1863.5	621.9	3.0
	$20Cu/ZrO_2$	69.3	12.6	80.9	2.3	2.5	0.9	0.2	0.6	1595.3	515.3	3.0
	$30Cu/ZrO_2$	68.8	14.5	78.4	2.6	2.5	1.0	0.3	0.7	1688.4	539.8	3.1
548	$5Cu/ZrO_2$	78.0	16.1	68.3	3.9	5.0	3.8	0.3	2.6	3742.3	942.1	3.9
	$10Cu/ZrO_2$	81.5	13.6	73.3	3.0	4.1	3.8	0.2	2.0	2398.1	1189.8	2.1
	$20Cu/ZrO_2$	81.3	13.2	76.2	2.7	2.2	3.2	0.4	2.1	1941.8	608.7	3.2
	$30Cu/ZrO_2$	80.7	15.0	73.6	2.9	2.5	3.5	0.4	2.1	1966.2	533.3	3.7

[a] Others: CO and CO_2. Abbreviations: ethanol conversion (X_{EtOH}); acetaldehyde (AcH); ethyl acetate (EtOAc); methyl ethyl ketone (MEK); crotonaldehyde (CROT); propanone (PROP); ethene (ETE) and products of condensation and dehydration (PCD).

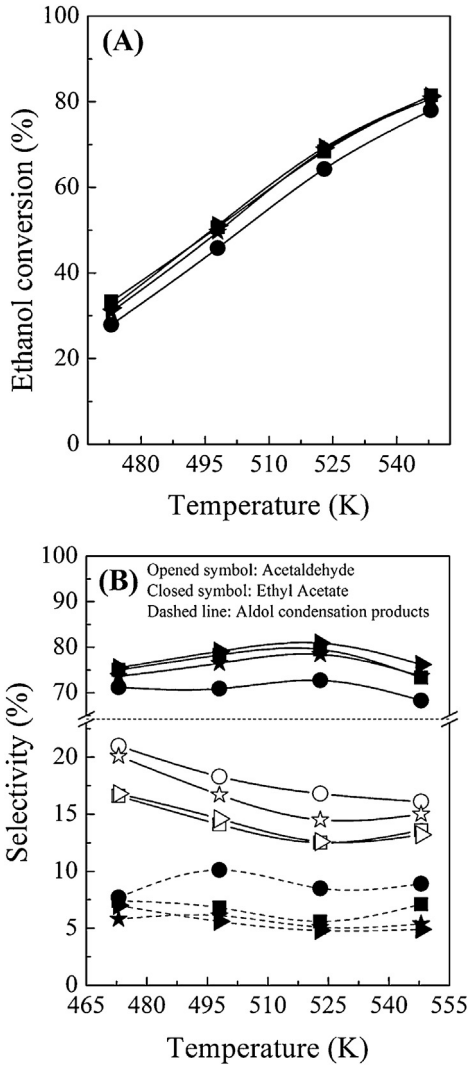

Fig. 6. Evolution of ethanol conversion (A) and selectivity to ethyl acetate, acetaldehyde and aldol condensation products (B) for Cu/ZrO_2 catalysts as a function of the reaction temperature: $5Cu/ZrO_2$ (●); $10Cu/ZrO_2$ (□); $20Cu/ZrO_2$ (►) and $30Cu/ZrO_2$ (⋆).

acetate for all samples is increasing with temperature enhancement from 473 to 523 K and after that is decreased (Fig. 6B).

The selectivity to acetaldehyde is the highest for catalyst with the lowest Cu content ($5Cu/ZrO_2$) at all reaction temperatures at the expense of ethyl acetate formation, followed by that of the catalyst with the highest Cu content ($30Cu/ZrO_2$) (Fig. 6B). Samples with 10 and 20 wt.% Cu show lower acetaldehyde product selectivity compared to that of other samples.

The selectivity to the sum of methyl ethyl ketone and crotonaldehyde (aldol condensation products) is the highest for $5Cu/ZrO_2$ catalyst at all reaction temperatures, especially, at temperature ≥498 K (Fig. 6). There is a low dependence of the condensation products selectivity on the reaction temperature for Cu/ZrO_2 catalysts with 20 and 30 wt.%.

Fig. 7 shows the rates of the formation of acetaldehyde and ethyl acetate as a function of the reaction temperature. At all reaction temperatures the $5Cu/ZrO_2$ catalyst demonstrates the lowest rates in the dehydrogenation of ethanol to ethyl acetate, whereas the $20Cu/ZrO_2$ sample exhibits the highest rate for ethyl acetate formation at temperature >473 K, followed by that of $10Cu/ZrO_2$ (Fig. 7B). The highest rate of acetaldehyde formation is observed for $5Cu/ZrO_2$ catalyst at reaction temperature ≥498 K (Fig. 7A). The rates of both products formation for all catalysts increase with increasing the reaction temperature.

The total amount of the products (designed as PCD) formed by aldol condensation (including MEK and CROT) and the product of ethanol dehydration (including ETE) is in parallel with the increase of reaction temperature for most of the samples with exception of $10Cu/ZrO_2$ (Table 4 and Fig. 8). All catalysts keep a specific relation between the formation of PCD and the water released during the reaction. The ratio H_2O/PCD is different for each catalyst. The highest amount of released water is observed for $5Cu/ZrO_2$ catalyst at temperature range 409–548 K, to which high amounts of PCD correspond (Table 4).

It should be to note, that the Cu/ZrO_2 catalysts showed relatively high stability of ethanol conversion and selectivity to different products formation during 25 h of work at all reaction temperatures (Figs. S1 and S2, see Supplementary material).

4. Discussion

XPS and DRIFTS data of adsorbed CO show that copper on reduced Cu/ZrO_2 samples presents in different oxidation state: Cu^0 and Cu^+. According to XPS analysis highly dispersed Cu^+ species are

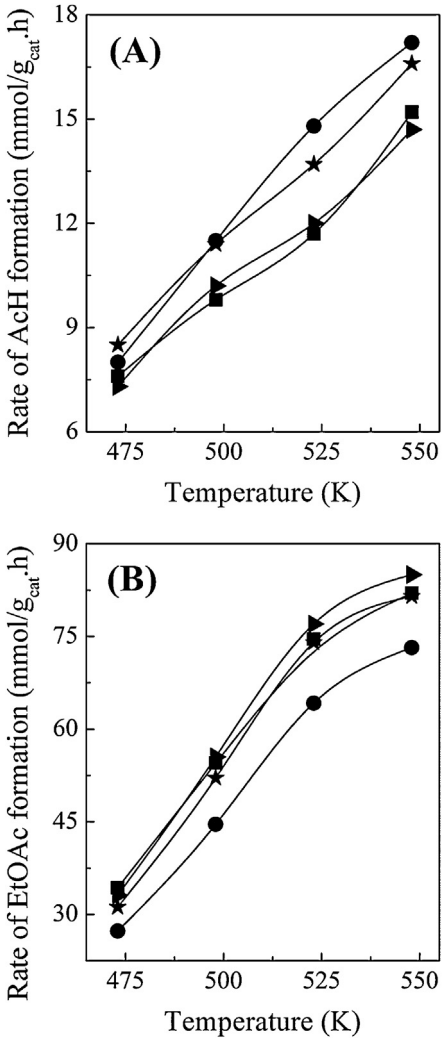

Fig. 7. Rate of the formation of acetaldehyde (A) and ethyl acetate (B) over Cu/ZrO_2 catalysts: $5Cu/ZrO_2$ (●); $10Cu/ZrO_2$ (□); $20Cu/ZrO_2$ (►) and $30Cu/ZrO_2$ (★).

observed on the surface of $5Cu/ZrO_2$, while Cu^0 is the prevailing species over samples with higher Cu content ≥20 wt.%. The presence of Cu^+ as dominant species is also supported by the lowest value of the metallic copper surface area in $5Cu/ZrO_2$, revealed by the N_2O data (Table 1). Some equilibrium between the Cu^0 and Cu^+ species for reduced $10Cu/ZrO_2$ is observed (Fig. 2B). The change of the proportion Cu^0/Cu^+ for supported Cu samples may be related to different reasons according to the literature [38,39]: (i) the decreased electron density of supported nanoparticles in respect to that of bulk metal; (ii) the change of the Cu—Cu coordination number of copper atoms owing to a high surface-to-volume ratio and (iii) the nature of interaction at the interface between supported metal and oxide support. Therefore, the changes of the electronic properties of copper have to be associated with one or more of these factors, which can be a function of the Cu content.

The interface between Cu and ZrO_2 of zirconia-supported Cu samples could be different in respect to the copper particle size and copper-oxide support contact structure. The presence of Cu^+ can be connected with the dispersion degree of supported Cu species. The increase of copper dispersion with decrease of Cu loading leads to an increase of the energy of Cu interaction with the support surface as well as to a decrease of the value of the Auger parameter, α_{Cu}. The lowest α_{Cu} value is detected for copper species in $5Cu/ZrO_2$ (1847.2 eV), to which corresponds the highest BE value of Cu $2p_{3/2}$ (932.5 eV) (Table 2). The shift of the valence band to a higher binding energy is a result of the reduced particle size [40] confirmed by the smallest Cu^0 particle size (3.1 nm) from the N_2O data (Table 1). The small particles or isolated Cu atoms in interface with the metal oxide support become electropositive charged, caused by the electron charge transfer from the metal to support [40]. It should be noted that the well dispersed copper oxide species is not easily reduced to metal due to the presence of oxygen vacancy in ZrO_2, which protects the interfacial Cu^+ from further reduction during catalytic reaction [41].

It has been shown that the copper-oxide support interface plays a significant role for the creation of oxygen sites. The formation of oxide species can occur not only at the metal-support interface but on the surface of copper nanoparticles according Ref. [42]. The last one could be caused by the oxygen transfer from the bulk ZrO_2 to copper surface, due to the high oxygen-rich interface generated by spillover mechanism between the copper and zirconia during the reduction process, similar to the observations for Cu/TiO_2 [43]. The high concentration of oxygen anions, characterizing the Cu/ZrO_2 samples, is revealed by the FTIR spectra of CO adsorption (Fig. 4). This suggests that the role of ZrO_2 support in the Cu/ZrO_2 system is to provide an extra charge to copper particles or oxygen to proximity of Cu. Even, the samples with relatively large Cu^0 particles can be characterized by the presence of surface adatoms, which are quite stable upon hydrogen reduction up to 573 K.

The results of catalytic test in the ethanol conversion reaction conclude that the product distribution is strongly influenced by the structure and electronic properties of supported copper particles and the surface acid-base properties of the catalysts as a function of the Cu content. Additionally, ethanol reaction gives an opportunity to obtain information about the electronic properties of Cu/ZrO_2 catalysts. It is well known that ethanol is converted via four main groups of reaction: dehydrogenation, dehydrogenation coupling, dehydration and hydrogenolysis. Dehydrogenation of ethanol forms acetaldehyde as a primary product. The consecutive aldol condensation of acetaldehyde yields *n*-butanol, crotonaldehyde and ketones. Dehydration reaction leads to the formation of diethyl ether and ethylene. It was reported [44] that the strong acidic sites are responsible for the dehydration reaction, whereas dehydrogenation requires moderate acid sites and strong basic sites.

Three different types of basic sites are detected over the surface of ZrO_2-supported copper catalysts: strongly basic surface O^{2-} ions, medium-strength Zr^{4+}—O^{2-} pairs and low-strength OH groups. Their relative concentration or density depends on the Cu content. The OH groups of ZrO_2 phase can be easily decomposed under increasing the reaction temperature and more oxygen anions and/or oxygen vacancies are formed. Whereas, *cus* $Zr^{\delta+}$ and Zr^{4+} cations attributed to the strong acid sites of Lewis type are stabilized on the surface of reduced Cu/ZrO_2 samples.

The high selectivity to acetaldehyde of $5Cu/ZrO_2$ catalyst can be associated with the presence of dominant Cu^+ species and the low basic sites density determined by the low strength of OH groups. The isolated copper ions can catalyze easy the ethanol dehydrogenation to acetaldehyde formation [45]. Therefore, the high rate of acetaldehyde formation of $5Cu/ZrO_2$ catalyst (Fig. 7A) could be related to the presence of oxygen near the well dispersed copper nanoparticles, which may facilitate the formation of ethoxide intermediate via O—H scission in ethanol molecule. It is well known [46] that the presence of oxygen facilitates the catalyst dehydrogenation activity. Similar to methanol activation on oxidized single-crystal Cu surfaces [47], the reactivity of ethanol to acetaldehyde can be greatly enhanced on the oxygen covered copper clusters, because the O—H bond scission is facilitated by the adsorbed oxygen. Surface science studies have also shown that the co-adsorbed oxygen on the surface of transition metals act as a Brönsted base to facilitate the O—H bond cleavage [46]. Subsequent C—H bond cleavage

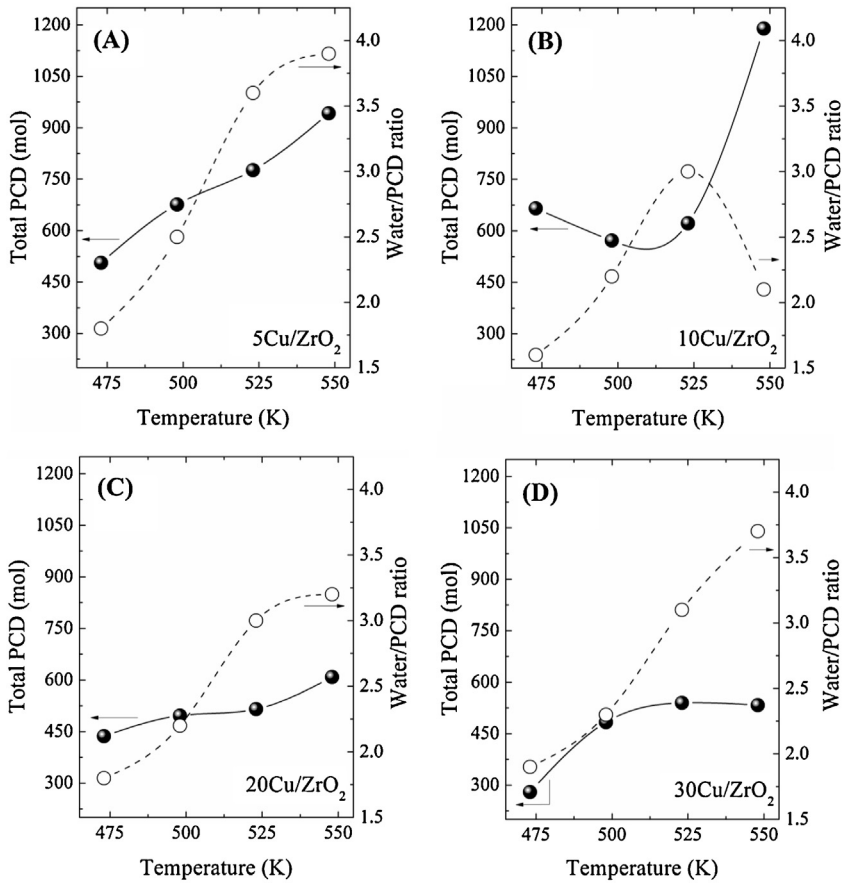

Fig. 8. Effect of the reaction temperature on the change of total PCD and ratio of water/PCD for $5Cu/ZrO_2$ (A), $10Cu/ZrO_2$ (B), $20Cu/ZrO_2$ (C) and $30Cu/ZrO_2$ catalyst (D).

leads to the formation of acetaldehyde or ketone, which can be also catalyzed by the presence of surface oxygen. The surface ethoxide intermediate can either loss hydrogen to produce acetaldehyde or pick up hydrogen to form ethanol and then decomposes to acetaldehyde. The dependence of the rate of alcohol dehydrogenation on the oxygen coverage copper was interpreted in terms of Langmuir type dependence on the oxygen surface coverage [48]. It can be concluded that the oxygen linked to copper nanoparticles in $5Cu/ZrO_2$ strongly affects the electron density of copper species.

The catalytic behavior of $5Cu/ZrO_2$ catalyst is also determined by the presence of strong Lewis acid sites (Zr^{4+}) that promotes the high selectivity to aldol condensation products (Fig. 6B). It has been shown [49] that the acetaldehyde condensation (β-aldolization) is promoted by the presence of basic sites to abstract of α-hydrogen atom and strong Lewis acid sites to bind the two molecules of acetaldehyde. The selectivity to methyl ethyl ketone and croton aldehyde for $5Cu/ZrO_2$ increases with the increase of reaction temperature from 473 to 498 K and after that is decreased with further increasing the reaction temperature (Fig. 6). The last one could be connected with the increase of the selectivity to dehydration products (Table 3). It is well known that the aldolization process is accompanied with a high amount of water released under reaction conditions. It is seen from the Fig. 8, that the highest amounts of released water for $5Cu/ZrO_2$ catalyst at reaction temperature ≥498 K correspond to the highest amounts of PCD. In addition, the ratio H_2O/PCD for the same catalyst also increases with increasing the reaction temperature (Fig. 8).

It is interesting to note, that the $30Cu/ZrO_2$ catalyst with the highest Cu content also shows a high selectivity to acetaldehyde (Fig. 6B). In the case of $30Cu/ZrO_2$ sample, the presence of oxygen sites near the bigger metal copper nanoclusters (12.6 nm) can be caused by the oxygen transfer from the ZrO_2 oxide substrate to copper surface, due to the oxygen-rich interface at supported metal-oxide support. However, the $30Cu/ZrO_2$ catalyst shows also a higher rate of ethyl acetate formation and a lower selectivity to condensation products in relation to that of $5Cu/ZrO_2$ (Figs. 6 and 7) due to the low basic sites density defined by the dominant Cu^0 and to the low degree of strong Lewis acid sites of Zr^{4+} ions covered by copper species, respectively.

The presence of Cu species with different electron density (Cu^0 and Cu^+) defined by XPS and the high concentration of basic sites (O^{2-}) detected by DRIFTS are responsible for the high rate of ethyl acetate formation for samples with Cu content ≥10 wt.%. It was proposed [7,17] that the coupling of aldehyde with alcohol or ethoxide species for ethyl acetate formation occurs over the mixed metal-oxides surface not over the Cu metal surface in Cu catalysts supported on Zn—Zr—Al—O system. The dehydrogenated ethanol or the acetaldehyde was adsorbed on the acid sites, while the hydrogen of the OH group in ethanol was abstracted by the surface base sites forming surface ethoxide [7,17]. Then a hemiacetal between these products is formed, which dehydrogenates very fast and produces ethyl acetate. It means that more active sites, like Cu^0 and Cu^+, will accelerate the acetal adsorption. Increasing the reaction temperature leads to the change of electron density of copper species and to increase of the oxygen sites transfer to copper metallic particles caused by the thermal decomposition of OH groups to oxygen anions or oxygen vacancies formation. This leads to the fast increase of the rate of ethyl acetate formation for all samples, being seen in Fig. 7B. However, depending on the oxygen resistance on the copper surface, its consumption by ethanol leads to the increase of acetaldehyde formation at temperature above 523 K. On the other hand, the fast consumption

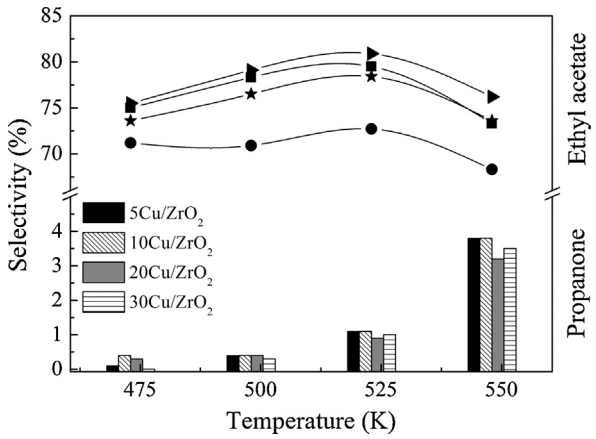

Fig. 9. Evolution of the selectivity to propanone and to ethyl acetate as a function of the reaction temperature for Cu/ZrO_2 catalysts: $5Cu/ZrO_2$ (●), $10Cu/ZrO_2$ (□), $20Cu/ZrO_2$ (►) and $30Cu/ZrO_2$ (★).

of acetaldehyde for condensation products formation accompanied by the high ratios of H_2O/PDC leads to a decrease of the ethyl acetate product formation at temperature range 523–548 K (Figs. 6 and 8).

It should be to note that the decrease of ethyl acetate formation for all catalyst at temperature above 523 K is in parallel with the increase of propanone formation in the temperature range of 523–548 K, being seen in Fig. 9. Different reasons may be proposed for the propanone formation. Similar to the observations in Ref. [50] propanone could be formed by the oxidation of acetaldol with the surface oxygen (O_s) adsorbed on $Cu/ZnO/Al_2O_3$ catalyst. The readily consumption of the oxygen for ethyl acetate and propanone formation may cause a loss of oxygen from the bulk ZrO_2, leading to a change of the electron density of surface copper species for ethyl acetate formation. Inui et al. [7] proposed that propanone is formed through a reverse of aldol addition of intermediate of propanone produced by dehydrogenation of ethanol. The loss of ethyl acetate formation at higher temperatures could be also related to the increase of the amount of condensation and dehydration products formation, as it was discussed above.

5. Conclusions

It is found that ZrO_2-supported Cu catalysts with different Cu content (5–30 wt.%) are active catalysts for dehydrogenation of ethanol. The results of XRD, N_2O decomposition and TPR data suggest a decrease of the copper metal dispersion with the increase of Cu content due to the strong particles agglomeration. It is shown that the catalytic properties of Cu/ZrO_2 catalysts are related to the specific electron density of supported Cu species defined by the particle size and the interface at metal-oxide support. The high selectivity to ethyl acetate formation of catalysts with Cu content $\geq$10 wt.% is determined by the high oxygen mobility from the bulk ZrO_2 to copper species causing a high density of basic sites (O^{2-}) and a more heterogeneous distribution of surface copper species (Cu^0/Cu^+) determined by DRIFTS of CO adsorption and XPS, respectively. The high density of Lewis acid sites defined by *cus* Zr^{4+} ions leads to the formation of by-products through aldol condensation.

Acknowledgments

The authors are gratefully acknowledged to FAPESP, CAPES, LNLS and CNPq for supporting this research.

Appendix A. Supplementary data

Supplementary data associated with this article can be found, in the online version, at http://dx.doi.org/10.1016/j.molcata.2013.09.038.

References

[1] J. Rass-Hansen, H. Falsig, B. Jørgensen, C.H. Christensen, J. Chem. Technol. Biotechnol. 82 (2007) 329–333.
[2] N.F. Zheng, G.D. Stucky, J. Am. Chem. Soc. 128 (2006) 14278–14280.
[3] B. Jorgensen, S.E. Christiansen, M.L.D. Thomsen, C.H. Christensen, J. Catal. 251 (2007) 332–337.
[4] Q.S. Meng, Y.L. Shen, J. Xu, J.L. Gong, Chinese J. Catal. 33 (2012) 407–415.
[5] X.M. Kong, L.L. Shen, Catal. Commun. 24 (2012) 34–37.
[6] P. Aghaei, R.J. Berger, Appl. Catal. B: Environ. 132 (2013) 195–203.
[7] K. Inui, T. Kurabayashi, S. Sato, N. Ichikawa, J. Mol. Catal. A: Chem. 216 (2004) 147–156.
[8] A.B. Sanchez, N. Homs, J.L.G. Fierro, P.R. de la Piscina, Catal. Today 107–08 (2005) 431–435.
[9] L.X. Wang, W.C. Zhu, D.F. Zheng, X. Yu, J. Cui, W.X. Zhang, Z.L. Wang, React. Kinet. Mech. Catal. 101 (2010) 365–369.
[10] A.B. Gaspar, F.G. Barbosa, S. Letichevsky, L.G. Appel, Appl. Catal. A: Gen. 380 (2010) 113–117.
[11] M.H. Zhang, G.M. Li, H.X. Jiang, J.Y. Zhang, Catal. Lett. 141 (2011) 1104–1110.
[12] R.Z. Li, M.H. Zhang, Y.Z. Yu, Appl. Surf. Sci. 258 (2012) 6777–6784.
[13] D.P. Volanti, A.G. Sato, M.O. Orlandi, J.M.C. Bueno, E. Longo, J. Andrés, Chem. Catal. Chem. 3 (2011) 839–843.
[14] F.-W. Chang, W.-Y. Kuo, K.-C. Lee, Appl. Catal. A: Gen. 246 (2003) 253–264.
[15] N. Iwasa, N. Takezawa, Bull. Chem. Soc. Jpn. 64 (1991) 2619–2623.
[16] K. Inui, T. Kurabayashi, S. Sato, J. Catal. 212 (2002) 207–215.
[17] K. Inui, T. Kurabayashi, S. Sato, Appl. Catal. A: Gen. 237 (2002) 53–61.
[18] A.B. Gaspar, A.M.L. Esteves, F.M.T. Mendes, F.G. Barbosa, L.G. Appel, Appl. Catal. A: Gen. 363 (2009) 109–114.
[19] P.C. Zonetti, J. Celnik, S. Letichevsky, A.B. Gaspar, L.G. Appel, J. Mol. Catal. A: Chem. 334 (2010) 29–34.
[20] A.G. Sato, D.P. Volanti, I.C. de Freitas, E. Longo, J.M.C. Bueno, Catal. Commun. 26 (2012) 122–126.
[21] D.P. Volanti, M.O. Orlandi, J. Andres, E. Longo, Cryst. Eng. Commun. 12 (2010) 1696–1699.
[22] S. Velu, K. Suzuki, C.S. Gopinath, H. Yoshida, T. Hattori, Phys. Chem. Chem. Phys. 4 (2002) 1990–1999.
[23] K.J. Soerensen, N.W. Cant, Catal. Lett. 33 (1995) 117–125.
[24] K.V.R. Charry, G.V. Sagar, C.S. Srikanth, V.V. Rao, J. Phys. Chem. B 111 (2007) 543–550.
[25] H. Wang, G. Li, Y. Xue, L. Li, J. Solid State Chem. 180 (2007) 2790–2797.
[26] P. Afanaiev, F. Geantet, M. Breysse, J. Catal. 153 (1995) 17–24.
[27] J. Sloczynski, R. Grabowski, A. Kozlowska, P.K. Olszewski, J. Phys. Chem. Chem. Phys. 5 (2003) 4631–4640.
[28] S. Ardizzone, C.L. Bianchi, Surf. Interface Anal. 30 (2000) 77–80.
[29] M.K. Dongare, A.M. Dongare, V.B. Tare, E. Kemniz, Solid State Ionics 455 (2002) 152–153.
[30] G.S. Wu, L.C. Wang, Y.M. Liu, Y. Cao, W.L. Dai, H.Y. He, K.N. Fan, Appl. Surf. Sci. 253 (2006) 974–982.
[31] A. Dandekar, M.A. Vannice, J. Catal. 178 (1998) 621–639.
[32] D. Bianchi, T. Chafik, M. Khalfallah, S.J. Teichner, Appl. Catal. A: Gen. 112 (1994) 57–73.
[33] G. Cerrato, S. Bordiga, S. Barbera, C. Morterra, Surf. Sci. 377–379 (1997) 50–55.
[34] K.T. Jung, A.T. Bell, J. Mol. Catal. 163 (2000) 27–42.
[35] K. Pokrovsky, K.T. Taek, A.T. Bell, Langmuir 17 (2001) 4297–4303.
[36] J.I. Di Cosino, V.K. Diez, M. Xu, E. Iglesia, C.R. Apesteguia, J. Catal. 178 (1998) 499–510.
[37] W.P. Dow, Y.P. Wang, T.J. Huang, J. Catal. 160 (1996) 155–170.
[38] J.A. Mejias, V.M. Jimenez, G. Lassaleta, A. Fernandez, J.P. Espinos, A.R. Gonzalez-Elipe, J. Phys. Chem. 100 (1996) 16255–16262.
[39] A. Barranco, F. Yubero, J.A. Mejias, J.P. Espinos, A.R. Gonzalez-Elipe, Surf. Sci. 482–485 (2001) 680–686.
[40] M. Rønning, F. Huber, H. Meland, H. Venvik, D. Chen, A. Holmen, Catal. Today 100 (2005) 249–254.
[41] W.P. Dow, T.J. Huang, J. Catal. 160 (1996) 171–182.
[42] R. Knapp, S.A. Wyrzgol, A. Jentys, J.A. Lercher, J. Catal. 276 (2010) 280–291.
[43] K. Varazo, F.W. Parsons, S. Ma, D.A. Chen, J. Phys. Chem. B 108 (2004) 18274–18283.
[44] M.E. Manriquez, T. Lopez, R. Gomez, J. Navarrete, J. Mol. Catal. A: Gen. 220 (2004) 229–237.
[45] J.L. Gole, M.G. White, J. Catal. 204 (2001) 249–252.
[46] K.Y. Guan, E.J.M. Hensen, Appl. Catal. A: Gen. 361 (2009) 49–56.
[47] J.N. Russel, S.M. Gates, J.T. Yates, Surf. Sci. 163 (1985) 516–540.
[48] B.A. Sexton, A.E. Hughes, N.R. Avery, Surf. Sci. 155 (1985) 366–386.
[49] A. Yee, S.J. Morrison, H. Idriss, Catal. Today 63 (2000) 327–335.
[50] D.J. Elliot, F. Pennella, J. Catal 119 (1989) 359–367.